View metadata, citation and similar papers at core.ac.uk

brought to you by CORE

provided by National Tsing Hua University Institutional Repository

Available online at www.sciencedirect.com

SCIENCE DIRECT®

ELSEVIER

Journal of Crystal Growth 269 (2004) 505–511

JOURNAL OF CRYSTAL GROWTH

www.elsevier.com/locate/jcrysgro

Growth of $Bi_2Sr_2Ca_{1-x}Pr_xCu_2O_y$ single crystals by traveling solvent floating zone method

K.W. Yeh[a,*], J.Y. Gan[a], Y. Huang[b]

[a] *Department of Materials Science and Engineering, National Tsing Hua University, Hsinchu, Taiwan*

[b] *Materials Science Center, National Tsing Hua University, Hsinchu, Taiwan*

Received 4 February 2004; accepted 27 April 2004

Available online 2 July 2004

Communicated by T. Hibiya

Abstract

A systematic study of $Bi_2Sr_2Ca_{1-x}Pr_xCu_2O_y$, where $x = 0-1.0$, was undertaken to determine growth parameters, crystal properties as well as the phase compositions. Single crystals were grown using the traveling solvent floating zone method. The dimension of single crystals with actual doping ratios x from 0.2 to 0.7 were typically 5 mm × 3 mm × 0.2 mm. Large single crystals of $Bi_2Sr_2PrCu_2O_y$ ($x = 1.0$), typically 10 mm × 3 mm × 0.2 mm, were successfully grown. These crystals contained no impurities and showed a clean X-ray diffraction pattern of the pure Bi-2212 phase. A planar interface was observed, indicating that a stable growth condition was established before zone quenching. As the Pr-doping level increased, the liquidus composition shifted pronouncedly to the corner of CuO in the pseudo-ternary $BiO_{1.5}$-(Sr,Ca,Pr)O-CuO phase diagram. Therefore, the solidus composition, $Bi_{1.965}Sr_{2.046}Pr_{1.096}Cu_{1.894}O_y$, and liquidus composition, $Bi_{2.17}Sr_{1.92}Pr_{0.31}Cu_{2.60}O_y$, were obtained by energy dispersive X-ray analyzer measuring.

© 2004 Elsevier B.V. All rights reserved.

PACS: 81.10.Fq; 74.72.Hs; 74.25.Dw; 47.20.Ma

Keywords: A1. Phase diagrams; A2. Traveling solvent zone growth; B1. Bi-2212; B2. Oxide superconducting materials

1. Introduction

$Bi_2Sr_2CaCu_2O_y$ (Bi-2212) has received extensive attention since the discovery of high-T_c superconductors [1–3]. Identifying the role of each constituent in superconducting compounds provides an indirect route of recognizing the origin of superconductivity. Among them, cation substitution of Ca in Bi-2212 compound has been studied extensively [4–18]. For example, it has been reported that the superconducting temperature of Bi-2212 was reduced by replacing Ca with other rare earth elements, such as Gd^{3+} [4,5], Ce^{3+} [6] and La^{3+} [7,8]. In particular, the Pr-substituted cuprate was found to show some anomalies on its antiferromagnetic transition temperature [9–11]. The real cause for such phenomenon has not been

*Corresponding author.

E-mail address: d867514@oz.nthu.edu.tw (K.W. Yeh).

0022-0248/$ - see front matter © 2004 Elsevier B.V. All rights reserved.
doi:10.1016/j.jcrysgro.2004.04.126

clearly identified because most of the polycrystalline Pr-doped Bi-2212 samples used in the studies are often found to be inhomogeneous [12–16].

More recently, some attention has been focused on the growth of single crystals. High-quality single crystals are indispensable for anisotropic physical measurements, such as CuO_2 interlayer coupling and carrier concentration. The studies by Sun et al. [17,18] have reported on the growth of $Bi_2Sr_2(Pr_xCa_{1-x})Cu_2O_y$ using a $BiO_{1.5}$-rich self-flux by the slow-cooling method and investigated the modulation and superconductivity of single crystals with actual doping levels $x = 0-0.78$. The studies indicated that as the doping level increased from $x = 0$ to 0.78, the crystal size decreased from 8 mm × 3 mm to 1 mm × 1 mm. Furthermore, with nominal compositions of doping level x greater than 0.7, the grown crystals are of the Bi-2201 and the Bi-2222 phase. Up to now, single crystals of higher Pr-doping ratios and complete substitution have not been obtained.

In this article, we report the growth of $Bi_2Sr_2(Pr_xCa_{1-x})Cu_2O_y$ single crystals by the traveling solvent floating zone (TSFZ) method. The TSFZ method prevented the high-temperature melt from reacting with the crucible. Moreover, at steady state, the melt zone will assume the liquid composition in equilibrium with the solid. Therefore, this technique provided a direct path to recognize the equilibrium liquidus composition by measuring the steady-state melt zone. In our earlier study, the same approach has been applied to define a $BiO_{1.5}$-rich primary crystallization field (PCF) of the $Bi_2Sr_2CaCu_2O_y$ compound [19,20]. Therefore, successfully growing the Pr-substituted Bi-2212 crystals would have to determine the equilibrium relations between the solidus and its corresponding liquidus of the phase diagram. This work, for the first time, obtained $Bi_2Sr_2(Pr_xCa_{1-x})Cu_2O_y$ single crystals of higher doping ratios and $Bi_2Sr_2PrCu_2O_y$ single crystals. It also identified the PCF of the Pr-doped Bi-2212 cuprate.

2. Experimental procedure

Single crystal growths were carried out in an infrared radiation furnace (model 15HD, NEC Nichiden Machinary) equipped with two 1.5 kW halogen lamps positioned at the foci of two ellipsoidal mirrors. The melt with a solvent composition was suspended by surface tension between the upper feed rod and lower seed rod (or solvent rod). Crystallization occurred at the growth front between the lower solvent rod and the melt and the seed crystal was formed in front of the lower rod. Crystal growth was then commenced when both rods were simultaneously lowered at the same rate. Adjusting the power of the lamps could precisely control the temperature of the molten zone. The crystal growths were carried out in an enclosed quartz tube where controlled oxygen pressures could be applied. Growth atmosphere in the chamber maintained constant at 1 atm, and low oxygen pressure was controlled by the flow of a mixed gas ($Ar:O_2 = 13:1$). The feed and seed rods rotated in opposite directions to provide well mixing in the molten zone.

The feed rods for the crystal growth were prepared by the conventional solid-state method. Nominal compositions of $Bi_{2.09}Sr_2(Pr_xCa_{1-x})Cu_{2.02}O_y$ and off-stoichiometric ratio $Bi_{0.325}Sr_{0.29}(Pr_xCa_{1-x})_{0.145}Cu_{0.24}O_y$ were varied in the range of $0 \leqslant x \leqslant 1.0$. Powder materials of 99.99% purity Bi_2O_3, $SrCO_3$, Pr_6O_{11}, $CaCO_3$ and CuO were mixed in an agate mortar for 12 h and then calcined at 800°C for 48 h with intermittent regrinding. The calcined mixture was reground into fine powders, pressed into a rubber tube under a hydrostatic pressure of 600 kg/cm^2 and sintered at 850°C for 48 h. Prior to the crystal growth run, the high density feed rod was obtained by zone-passing the rod at a rapid rate of 20 mm/h, then the solid–liquid interface could be held more stable during the succeeding crystal growth process because a penetration of the molten liquid into the grain boundaries of the feed rod was reduced. After growth stabilized at a slow growth rate of 0.2 mm/h and several centimeters of crystal was obtained, the lamp power was switched off to quench the molten zone.

A Rigaku Rotaflex RU-300 X-ray powder diffractometer with CuK_α X-ray source was used to investigate the phase purity and the lattice constant of crystals. The c-axis length of the

crystal was estimated by the Nelson–Riley extrapolation [21] with 2θ values of (0 0 $\underline{2}$ 0), (0 0 $\underline{2}$ $\underline{2}$), (0 0 $\underline{2}$ 6), (0 0 $\underline{2}$ $\underline{8}$) and (0 0 $\underline{3}$ $\underline{0}$) diffraction peaks. This extrapolation procedure gave an accuracy of better than 0.001 Å. The quantitative analyses were calibrated with an amorphous material (as prepared by splat-quenching) as the standard, with the nominal composition $Bi_2Sr_2(Pr_{0.5}Ca_{0.5})Cu_2O_y$. An inductively coupled plasma atomic emission spectrometer (ICP-AES) analyzer (Perkin-Elmer 300DV) was used to measure the quenched zone compositions. The concentration of the well-mixed nitric solution was optimized for fitting the ionic concentration of each element into the linear measurement range. The accuracy of the ICP-AES measurement is within 3% of the amount present. To further reveal the surface morphology as well as the compositions, a Joel JSM-840A high-resolution scanning electron microscope equipped with Link MK6B energy dispersive X-ray analyzer (EDX) was utilized. The characteristic peaks of each element, Bi^{3+}-L_α, Sr^{2+}-L_α, Pr^{3+}-L_α, Ca^{2+}-K_α, and Cu^{2+}-K_α were chosen. And in doing so, a relative error of less than 2% was obtained.

3. Results and discussion

3.1. Crystal growth and characterization

In the growth experiments, the $Bi_{2.09}Sr_2(Pr_x$-$Ca_{1-x})Cu_{2.02}O_y$ and off-stoichiometric ratio $Bi_{0.325}Sr_{0.29}(Pr_xCa_{1-x})_{0.145}Cu_{0.24}O_y$ were, respectively, selected as the starting feed and the solvent compositions. For comparison, a typical example in preliminary studies of the $Bi_2Sr_2CaCu_2O_y$ ($x = 0$) growth [20] is listed as the run number C0 in Table 1. Run numbers from P1 to P5 in Table 1 represent, respectively, the growths of the doping ratio $x = 0.1$, 0.2, 0.5, 0.7 and fully substituted $x = 1.0$. A series of single crystals, typically 5 mm × 3 mm, containing no impurities as verified by X-ray diffraction and EDX measuring, were successfully grown. This work for the first time obtained $Bi_2Sr_2(Pr_xCa_{1-x})Cu_2O_y$ single crystals of higher doping ratios ($x > 0.7$) and $Bi_2Sr_2PrCu_2O_y$ single crystals.

Table 1
Nominal compositions in the feed rod and the solvent rod of the initial conditions, and the actual compositions of single crystals and in the quenched zone in the $Bi_2Sr_2Ca_{1-x}Pr_xCu_2O_y$ compound

Run no.	Nominal x-value	Nominal compositions								Actual compositions								Crystal x-value
		Feed (normalized to 7)				Solvent (mol%)				Crystal (mol%)				Quenched zone (mol%)				
		Bi	Sr	Ca	Pr	Cu	Bi	Sr	Ca	Pr	Cu	Bi	Sr	Ca	Pr	Cu	Bi	Sr	Ca	Pr	Cu	
C0	0	2.09	2.00	0.89	0	2.02	32.5	29.0	14.5	0	24.0	30.66	26.64	13.73	0	28.97	34.65	27.30	11.53	0	26.52	0
P1	0.1	2.09	2.00	0.80	0.09	2.02	32.5	29.0	14.5	0	24.0	29.60	28.56	11.67	2.94	27.23						0.20
P2	0.2	2.09	2.00	0.71	0.18	2.02	32.5	29.0	11.6	2.9	24.0	29.33	28.54	9.90	4.92	27.31	33.14	27.49	9.59	0.50	29.28	0.33
P3	0.5	2.09	2.00	0.44	0.45	2.02	32.5	29.0	7.2	7.3	24.0	28.75	27.54	5.72	10.90	27.09	32.74	27.13	6.78	1.97	31.37	0.66
P4	0.7	2.03	2.05	0.31	0.71	1.90	32.2	29.0	1.6	3.6	33.6	27.55	27.88	5.24	12.69	26.64						0.71
P5	1.0	2.09	2.00	0	0.89	2.02	32.5	29.0	0	14.5	24.0	28.98	29.26	0	14.65	27.11	30.96	27.41	0	4.45	37.18	1.0
P6	1.0	2.03	2.05	0	1.02	1.90	31.0	27.4	0	4.4	37.2	28.07	29.23	0	15.65	27.05	32.33	27.76	0	4.93	34.98	1.0

However, after observing the cross-section of the quenched zone by a stereoscope, the freezing interface of P5 ($x = 1.0$) did breakdown into a cellular interface. The composition of the quenched zone was analyzed by examining the axial cross-section. After the growth, the melt composition significantly changes to a CuO-rich composition of $Bi_{0.308}Sr_{0.281}Pr_{0.042}Cu_{0.369}O_y$. In order to achieve steady-state growth, this highly CuO-rich composition of $Bi_{0.308}Sr_{0.281}Pr_{0.042}Cu_{0.369}O_y$ was selected for the solvent rod, and the crystal composition of $Bi_{2.029}Sr_{2.048}Pr_{1.025}Cu_{1.897}O_y$ was selected for the feed rod. After P6 growth, in which a constant shape and volume of the zone was maintained, larger crystals of approximately 10 mm × 3 mm were produced with significantly improved crystallinity. Typical single crystals of $x = 1.0$ are shown in Fig. 1. The growth front was planar, which indicated that a stable growth condition had been established before zone quenching. The composition of the quenched zone was measured to be $Bi_{0.323}Sr_{0.278}Pr_{0.049}Cu_{0.350}O_y$, close to the nominal one. Besides, the crystal composition of $Bi_{1.965}Sr_{2.046}Pr_{1.096}Cu_{1.894}O_y$ was almost identical to the nominal composition of feed rod within the error of EDX technique. It is suggested that steady-state growth conditions are established; consequently, this CuO-rich melt would correspond to the nominal liquidus, which is in a tie-line relationship with the crystalline solidus in the Pr2212 system. It is noteworthy that the precise control of the solvent compositions is critical for stabilizing the growth interface as well as enhancing the purity of the crystallized phase.

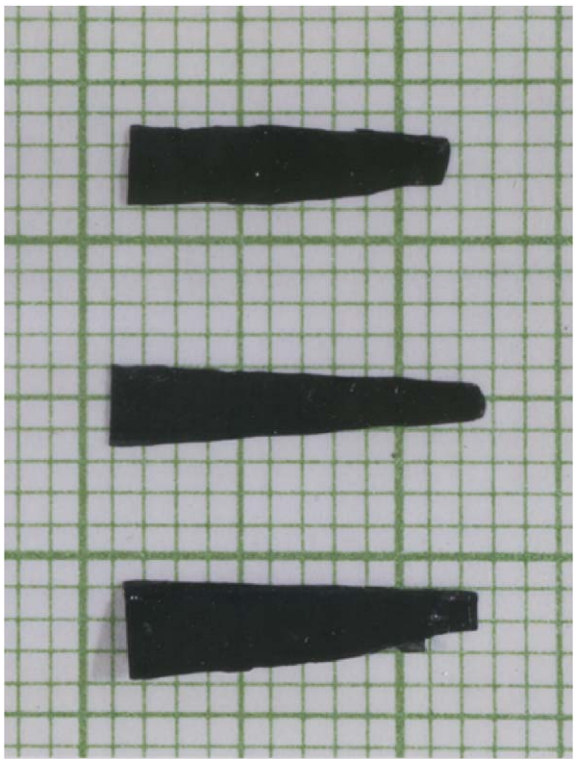

Fig. 1. A photograph of some $Bi_2Sr_2PrCu_2O_y$ single crystals. The actual size of a square in the background is 1 mm × 1 mm.

EDX measurements, both in parallel and perpendicular to growth axis of some P1 and P2 crystals with lower doping levels ($x = 0.2-0.33$), revealed that the concentrations of Bi, Sr and Cu were uniform. Among 20 sampling points of every 100 μm spacing, the standard deviation of each element was within 1.5%. However, deviations were more than 20% for both the Ca and Pr contents in the direction of the growth axis. In the experiments of low x-value, the Pr ionic content changed significantly in front of the growth interface. On the other hand, in those experiments with x-value larger than 0.5 (P3, P4) and equaling 1.0 (P5, P6), the compositional discrepancies of all elements in the compound were all less than 2%. Therefore, crystals displayed excellent uniformity and crystallinity. A striking feature here is that crystal growths of higher doping ratio were much more stable than those of lower doping ratio, and at the same time the crystal quality of the former is better than that of the latter.

A significant difference between nominal and crystal compositions with respect to Ca/Pr ratio can be observed from the column of the crystal composition in Table 1. The crystal x-value was obviously larger than the nominal x-value, and this tendency was similar to the previous reports [17]. Moreover, the Cu content of the Pr-doped crystals was observed at about 27 mol% and displayed a large difference of 1–2 mol% lower than the undoped crystals. The Bi content in the higher doping crystals was also deficient compared to that in lower Pr-doping crystals. These above results would suggest the possibility that Pr atom,

which has a smaller ionic radius, could occupy some Cu and even Bi atomic sites, and gained easier entry into the BiO-SrO-CaO-CuO layer structure than Ca atoms.

The X-ray diffraction pattern of the $Bi_2Sr_2PrCu_2O_y$ single crystals is plotted in Fig. 2. In this plot, only (0 0 l) diffraction lines appear. No peaks of impurities such as the Bi-2201 are observed, thus displaying a single crystalline Bi-2212 phase. Hence, using a fitting method with the Nelson–Riley function, the c-axis length was estimated as 30.345 Å. The relations of Pr-doping ratio x and the crystal c-axis length are then plotted in Fig. 3. Except for the larger distributions at $x = 0$, which indicates a larger solid-solution range of the $Bi_2(Sr, Ca)_3Cu_2O_y$ compound [20], the data show a simple regression $y = 30.8860 - 0.5413x$, displaying a linear decrease of the c-axis length as the Pr-doping level x increases. However, contrary to the results of Sun et al. [17], their crystals display a larger slope at higher doping levels ($x = 0.45-0.78$). The anomalous features in the change of structural parameters c with the Pr content ($x = 0-0.78$) were observed to have a jump at $x = 0.45$. The reason is required for clarifying, nonetheless, from our compositional point of view, that the unstable growth experiments with higher Pr-doping levels by the slow-cooling method were due to the unsuitable $BiO_{1.5}$-rich flux compositions. The detailed compositional range will be discussed in Section 3.2.

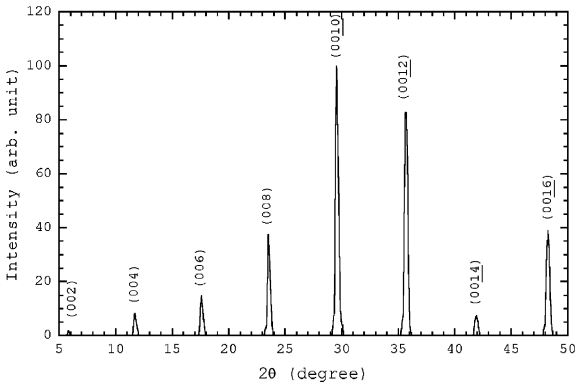

Fig. 2. A typical X-ray diffraction pattern of a $Bi_2Sr_2PrCu_2O_y$ single crystal. By the Nelson–Riley calibration, the corresponding lattice spacing d value of each (0 0 l) diffraction peak was extrapolated the diffraction angle θ to 90°, and then the c-axis length of this single crystal was estimated equaling 30.345 Å.

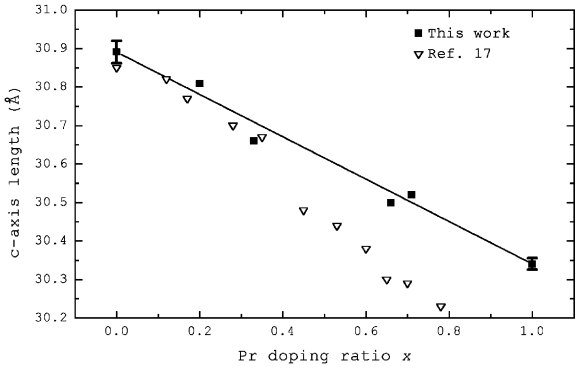

Fig. 3. Linear dependence of the c-axis length with Pr-doping ratio x for the $Bi_2Sr_2(Ca_{1-x}Pr_x)Cu_2O_y$ single crystals. For crystals at $x = 0$ and 1.0, the solid rectangles represent the average and the error bars represent the standard deviation. The standard deviation equals around 0.015 Å of $x = 1.0$ and 0.03 Å of $x = 0$. The open triangles stand for the results of Sun et al. [17].

3.2. The investigation of phase diagram

A precise quantitative analysis is required for analyzing the phase diagram. Both the EDX and ICP quantitative analyses were specifically calibrated by an amorphous standard with a nominal composition of $Bi_{2.09}Sr_2(Pr_{0.5}Ca_{0.5})Cu_{2.02}O_y$. It should also be noted that in measuring the quenched zone composition that is fairly distant from the solid-solution region, the compositional differences between EDX and ICP were within 3%. For purposes of discussion, a representation of the equilibria will take the form of the pseudo-ternary composition triangle shown in Fig. 4, composed of the isothermal section $BiO_{1.5}$-(Sr,Ca, Pr)O-CuO at approximately 900°C. This triangle has, as two of its vertices, $BiO_{1.5}$ and CuO. The third vertex represents the combined concentration of SrO, CaO and PrO. The compositional distributions in crystal, as described in Section 3.1, displayed lower Cu and Bi contents with higher x.

The composition of the molten zone, starting from a nominal composition, gradually adjusted to PCF as the zone stabilized in a controlled TSFZ growth. Starting with a $BiO_{1.5}$-rich and

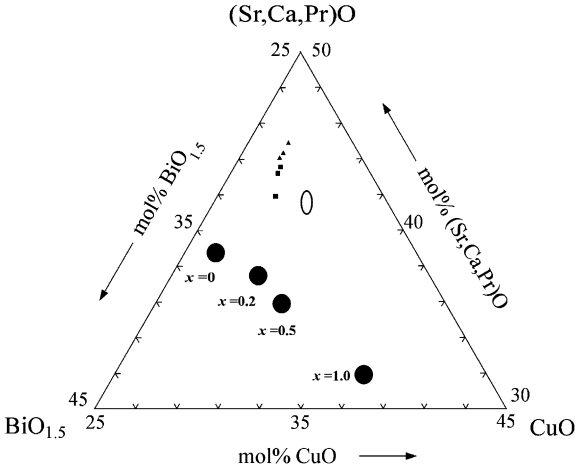

Fig. 4. The pseudo-ternary (Sr,Ca,Pr)O-$BiO_{1.5}$-CuO phase diagram of the $Bi_2Sr_2(Ca_{1-x}Pr_x)Cu_2O_y$ oxide system. The ellipse represents the solid-solution region of the $Bi_2Sr_2CaCu_2O_y$ [20]. Crystals with high doping levels ($x > 0.5$) were displayed as solid triangles, and crystals with lower doping levels were displayed by solid rectangles. The large solid circles represent the quenched zone compositions of each nominal doping level x (0.2, 0.5 and 1.0). By comparing between ICP and EDX analysis, the center of solid circles represents the average composition, and the diameter of the solid circles stands for the deviation.

CuO-deficient composition in the phase diagram, both ICP and EDX results indicated that while the Pr-doping level x increased, the corresponding liquidus composition shifted pronouncedly to the $BiO_{1.5}$ and CuO-rich side of the phase diagram. The trace, from the starting solvent to PCF of 22Pr2, is clearly shown in Fig. 4. Furthermore, when x increased, the Bi content decreased slightly while Cu concentration showed a pronounced increase. Therefore, the greatly differed compositional variation between the nominal and the quenched zone in P5 growth ($x = 1.0$) may account for the thinner grain cells at the growth interface and instabilities during crystal growth. It should be pointed out again that after using the equilibrium solvent composition $Bi_{2.17}Sr_{1.92}Pr_{0.31}Cu_{2.60}O_y$ in P6 growth, a nearly planar growth interface was obtained. Besides, the composition in the quenched zone was close to the nominal one. This compositional range around $Bi_{2.17}Sr_{1.92}Pr_{0.31}Cu_{2.60}O_y$ should be relatively close to the PCF for the $Bi_2Sr_2PrCu_2O_y$ compound. The detailed compositions of the quenched zone with different x are listed in Table 1. This compositional range, which has been normally considered with a higher melting point, was determined to have mixed phases consisting of Bi-2212, Bi-2201 and CuO [22,23]. A striking feature here is that in the Pr2212 systems, we propose CuO-rich PCFs as eutectics with lower melting points.

It was interesting to note that the Pr concentration (P2, P3, P5) remaining in the molten zone was much lower than the nominal one. One possible reason could be that the large segregation coefficient ($k_{Pr} = 3.29$) led to a higher Pr concentration in crystal than in the molten zone. This significant compositional difference may gave resulted in the fluctuation of Pr atomic concentration in front of the freezing interface, and thereby led to the axial uniformity of as-grown crystals. As previously mentioned in our observations, this phenomenon also seriously affected the stability of the crystal growth, especially that of smaller x-values. Replacing the feed rod's composition obtained from the as-grown crystal of P5, the stability was established in P6 growth ($x = 1.0$) and by doing so, the Pr mole ratio of the melt zone (4.925%) was found close to the nominal one (4.451%). Therefore, it suggests that thorough understandings of the PCF of varied doping levels are necessary for the successful growth of high-quality crystals.

4. Conclusions

For the growth of large single crystals of Bi-2212 family with a homogeneous composition and uniform physical properties, developments of a reproducible growth method and investigation of the phase diagram are crucial. High-quality single crystals of $Bi_2Sr_2(Pr_xCa_{1-x})Cu_2O_y$ of approximately 5 mm × 3 mm × 0.2 mm and single crystals of $Bi_2Sr_2PrCu_2O_y$ ($x = 1.0$) of typically 10 mm × 3 mm × 0.2 mm were obtained from the TSFZ-grown boule. The solvent composition within the melt in the TSFZ experiments would approach the liquidus composition that corresponds to the grown crystal at a steady state. The primary crystallization fields relative to Bi-2212 solid-solution region were found to locate nearer

to the $BiO_{1.5}$ and CuO-rich side in the phase diagram. At a sufficiently slow growth rate, a stable composition within the zone and a planar growth front were maintained at a stable crystallization temperature. Larger crystals of better quality can thus be obtained.

Acknowledgements

The authors would like to thank the National Science Council of the Republic of China for financially supporting this work. Suggestions provided by professors M.K. Wu and H.C. Ku are greatly appreciated.

References

[1] J.G. Bednorz, K.A. Müller, Z. Phys. B 64 (1986) 189.
[2] M.K. Wu, J.R. Ashburn, C.J. Torng, P.H. Hor, R.L. Meng, L. Gao, Z.J. Huang, Y.Q. Wang, C.W. Chu, Phys. Rev. Lett. 58 (1987) 908.
[3] H. Maeda, Y. Tanaka, M. Fukutomi, T. Asano, Jpn. J. Appl. Phys. 27 (1988) L209.
[4] N. Sanada, T. Nakadaira, M. Shimomura, Y. Suzuki, Y. Fukuda, M. Nagoshi, Y. Syono, M. Tachiki, Physica C 263 (1996) 286.
[5] A.J.S. Choudhury, N.R. Charnley, F.R. Wondre, A.V. Volkozub, P.A.J. de Groot, B.M.R. Wanklyn, J.W. Hobby, J. Crystal Growth 169 (1996) 405.
[6] H. Jin, N.L. Wang, Y. Chong, M. Deng, L.Z. Cao, Z.J. Chen, J. Crystal Growth 149 (1995) 269.
[7] J. Fujikami, R. Yoshizaki, M. Akamatsu, T. Ishigaki, H. Asano, Physica C 174 (1991) 359.
[8] H. Jin, J. Kötzler, Physica C 325 (1999) 153.
[9] H.C. Ku, T.I. Hsu, Y.Y. Hsu, T.J. Lee, K.W. Yeh, Y. Huang, J.Y. Lin, S.J. Chen, H.D. Yang, Y.Y. Chen, J.C. Ho, X.G. Li, Chin. J. Phys. 35N6-2 (1997) 90.
[10] C.L. Yang, J.H. Shieh, Y.Y. Shu, H.C. Ku, J.C. Ho, Phys. Rev. B 52 (1995) 10452.
[11] H.C. Ku, Y.B. You, S.R. Sheen, Y.M. Wan, T.I. Hsu, Y.Y. Hsu, J. Low Temp. Phys. 105 (1996) 1463.
[12] C. Quitmann, D. Andrich, C. Jarchow, M. Fleuster, B. Beschoten, G. Güntherodt, V.V. Moshchalkov, G. Mante, R. Manzke, Phys. Rev. B 46 (1992) 11813.
[13] C. Kendziora, L. Forro, D. Mandrus, J. Hartge, P. Stephens, L. Mihaly, R. Reeder, D. Moechar, M. Rivers, S. Sutton, Phys. Rev. B 45 (1992) 13025.
[14] V.P.S. Awana, L. Menon, S.K. Malik, Phys. Rev. B 51 (N14) (1995) 9379.
[15] X.L. Chen, J.K. Liang, J.R. Min, J.Q. Li, G.G. Rao, Phys. Rev. B 50 (N5) (1994) 3431.
[16] Y. Takano, K. Morita, H. Ozaki, K. Sekizawa, J. Magnetism, Magn. Mater. 140–144 (1995) 1343.
[17] X. Sun, X. Zhao, W. Wu, X. Fan, X.-G. Li, Physica C 305 (1998) 227.
[18] X. Sun, X. Zhao, W. Wu, X. Fan, X.-G. Li, H.C. Ku, Physica C 307 (1998) 67.
[19] Y. Huang, M.H. Huang, K.W. Yeh, M.Y. Hong, Mater. Chem. Phys. 41 (1995) 290.
[20] Y. Huang, M.H. Huang, J.M. Jian, J. Crystal Growth 166 (1996) 867.
[21] B.D. Cullity, Elements of X-ray Diffraction, 2nd Edition, Addison-Wesley, Reading, MA, 1978, p. 356.
[22] B. Hong, J. Hahn, T.O. Mason, J. Am. Ceram. Soc. 73 (1990) 1965.
[23] Y. Idemoto, S. Kobayashi, K. Fueki, Physica C 229 (1994) 47.